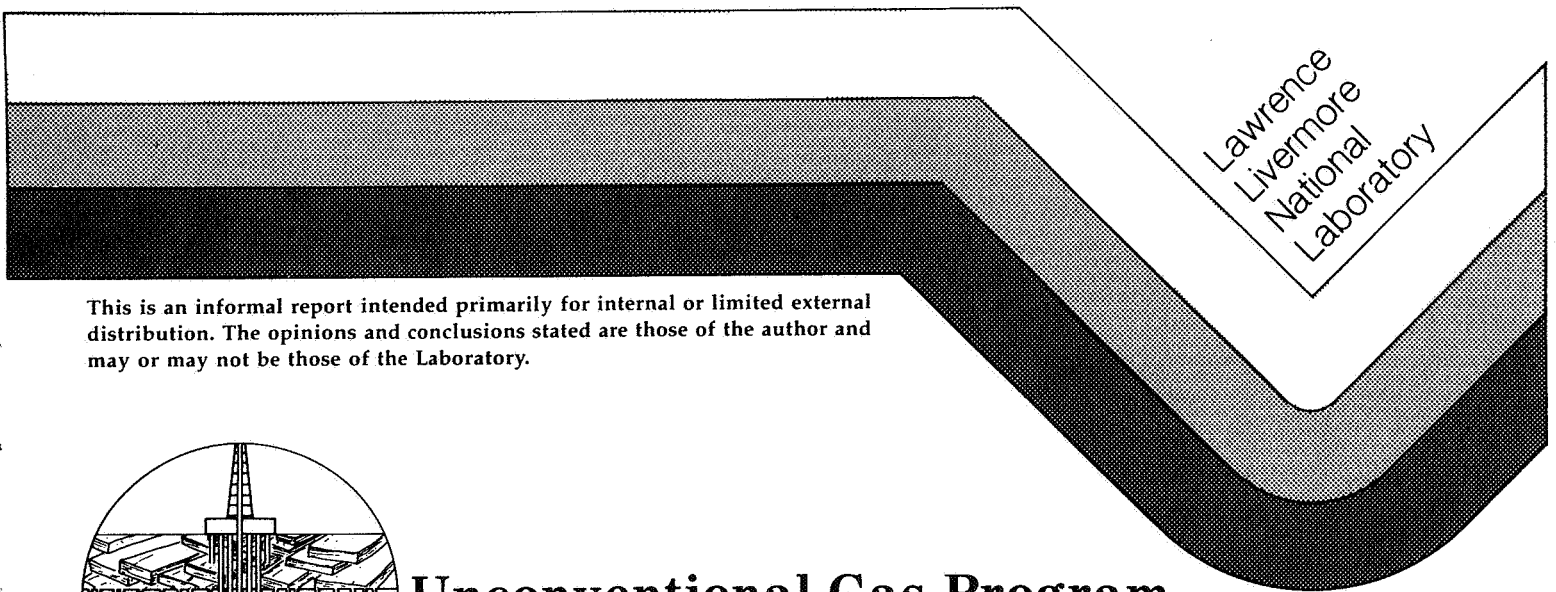


# High-Pressure Mechanical and Sonic Properties of a Devonian Shale from West Virginia

H. C. Heard  
W. Lin

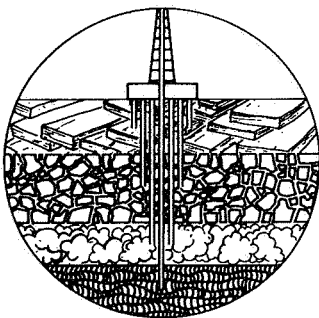
Prepared for  
Morgantown Energy Technology Center  
Morgantown, WV

January, 1986



Lawrence  
Livermore  
National  
Laboratory

This is an informal report intended primarily for internal or limited external distribution. The opinions and conclusions stated are those of the author and may or may not be those of the Laboratory.



## Unconventional Gas Program

Eastern Devonian Shales Research

**DISCLAIMER**

This document was prepared as an account of work sponsored by an agency of the United States Government. Neither the United States Government nor the University of California nor any of their employees, makes any warranty, express or implied, or assumes any legal liability or responsibility for the accuracy, completeness, or usefulness of any information, apparatus, product, or process disclosed, or represents that its use would not infringe privately owned rights. Reference herein to any specific commercial products, process, or service by trade name, trademark, manufacturer, or otherwise, does not necessarily constitute or imply its endorsement, recommendation, or favoring by the United States Government or the University of California. The views and opinions of authors expressed herein do not necessarily state or reflect those of the United States Government or the University of California, and shall not be used for advertising or product endorsement purposes.

Printed in the United States of America  
Available from  
National Technical Information Service  
U.S. Department of Commerce  
5285 Port Royal Road  
Springfield, VA 22161

<u>Price Code</u>	<u>Page Range</u>
A01	Microfiche
<u>Papercopy Prices</u>	
A02	001-050
A03	051-100
A04	101-200
A05	201-300
A06	301-400
A07	401-500
A08	501-600
A09	601

INDEX

	PAGE
ABSTRACT .....	ii
1. INTRODUCTION .....	1
2. EXPERIMENTAL TECHNIQUE .....	4
3. RESULTS .....	5
3.1 Pressure-Volume .....	5
3.2 Triaxial stress, compression .....	7
3.3 Triaxial stress, extension .....	12
3.4 Uniaxial strain, compression .....	12
3.5 Tensile strength .....	16
3.6 Acoustic velocities and dynamic elastic constants .....	16
4. APPENDIX: Tabulated data of all tests .....	24
5. REFERENCES .....	39
6. ACKNOWLEDGMENTS .....	41

Uniaxial strain loading in compression of members B, C and D resulted in a large hysteresis between the loading and unloading cycles in each material, similar to behavior exhibited by most rocks. Loading perpendicular to bedding resulted in a stress path which follows the extension failure envelope to low-moderate pressure, then progressively deviates below it as pressure is increased. Loading parallel to bedding indicated a path above the extension envelope at low pressure, then crossing it and becoming lower at high pressure. In two of the three members tested, the loading envelope remained at  $\sim 1/2$  the shear stress characteristic of the compression failure envelope.

The tensile strength was found to be anisotropic for all four members. Strength perpendicular to bedding was about one-half that for parallel to bedding. Little difference is apparent between members.

The behavior of compressional and shear wave velocities determined both parallel and perpendicular to bedding in all four shale members were quite consistent as pressure was increased. All velocities strongly increase up to about 0.2 GPa, then become almost constant to 1.0 GPa. This is consistent with crack closure at low pressure. Strong anisotropies are shown among the several compressional and shear modes. All data indicate these shales are approximately transversely isotropic. Elastic moduli were calculated for each unit. Comparison of these data suggest that units A and C are closely similar in behavior as are units B and D. This is consistent with most other observations.

## 1. INTRODUCTION

This research was performed as part of the Unconventional Gas Program at LLNL (1). It is estimated that tight (low permeability) Eastern Devonian gas shales and Western gas reservoirs contain large quantities of natural gas, but because of the low production rates, these resources are difficult and uneconomic to recover (2). Current methods of enhancing permeability in these gas-bearing formations include dynamic stimulation with propellants or chemical explosives, and fracturing the formations hydraulically. Empirical applications of these methods have given variable results and thus demonstrate that the physics of permeability enhancement are not well understood. Much progress has been forthcoming recently in the theoretical area and improved predictive numerical models have resulted (3-8). The goal of these studies is to predict such parameters as fracture intensity, geometry and extent as well as porosity and permeability enhancement. In order to take maximum advantage of this approach, equation of state (EOS) and mechanical property measurements of the reservoir rocks are required. For numerical modeling of explosive stimulation, EOS data at very high pressures are needed. This report presents the results of our static mechanical measurements and sonic velocities on a particular Devonian shale at such pressures.

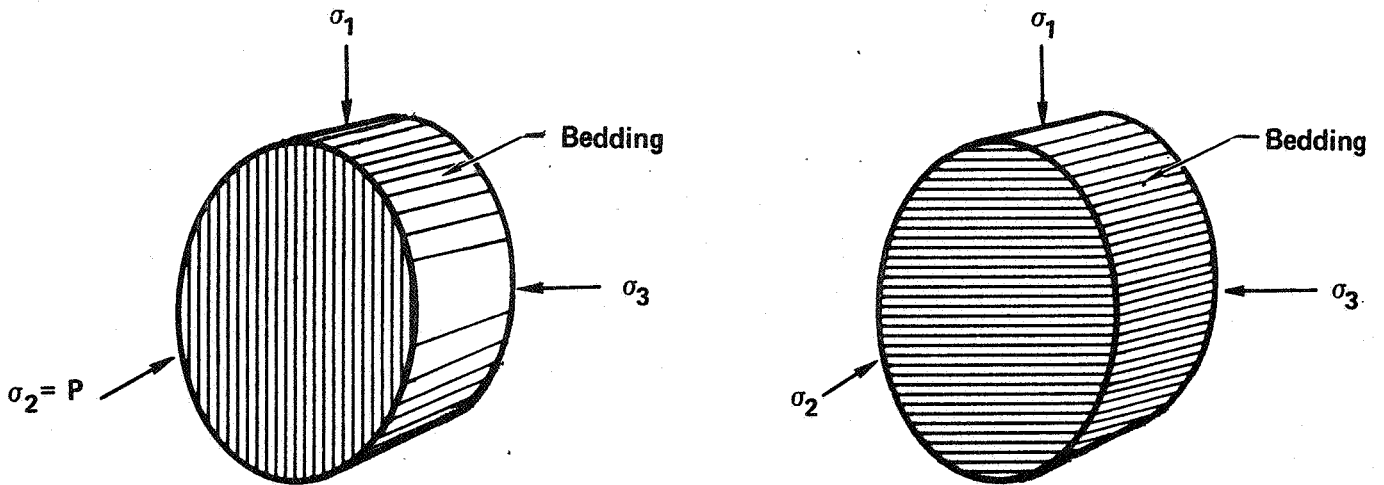
The starting material was a 10 cm diameter drill core of Devonian shale from the Columbia Gas Transmission Company's well 20403, Huntington, West Virginia. The geologic section has been divided into four distinct shale units at the indicated depths:

- A) Upper gray member: 807-1039 m
- B) Brown gaseous member: 1039-1116 m
- C) Olentangy white member: 1116-1203 m
- D) Marcellus black member: 1203-1233 m

The mechanical behavior, was then determined for each individual member. Six types of tests were performed on cylindrical samples of each material as illustrated in Figures 1a and 1b:

1. Quasihydrostatic pressure-volume (P-V) to 4.0 GPa
2. Compressive strength in triaxial stress loading at confining pressures

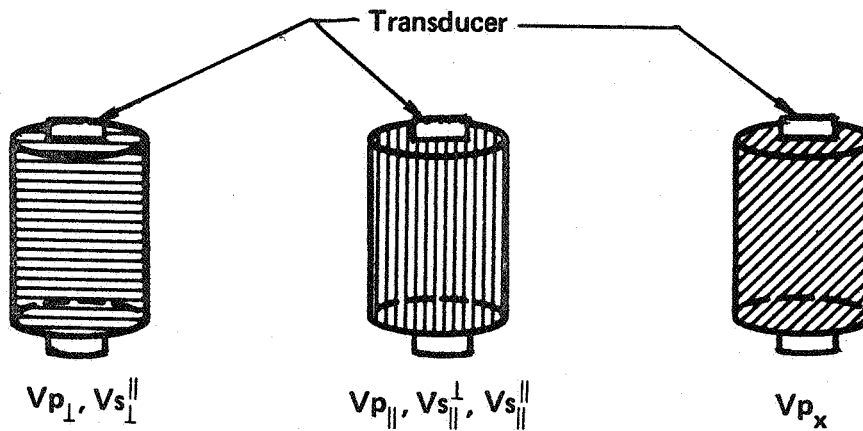
(c)



Test type

5) Indirect tensile (Brazilian test)  $\sigma_1 > \sigma_2 = P = 0.1 \text{ MPa} > \sigma_3$

(d)



$V_{p\perp}$ ,  $V_{p_x}$ , and  $V_{p\parallel}$  are P-waves propagating  $\perp$ ,  $45^\circ$ , and  $\parallel$  to bedding respectively.

$V_{s\perp}^{\parallel}$  is S-wave propagating  $\perp$  to bedding, polarized  $\parallel$  to bedding.

$V_{s\parallel}^{\perp}$  and  $V_{s\parallel}^{\parallel}$  are S-waves propagating  $\parallel$  to bedding, polarized  $\perp$  and  $\parallel$  to bedding respectively.

Test type

6) Compressional and shear wave velocity determinations.

Figure 1 (cont.): Test Set-Ups for Tensile and Sonic Properties Tests

thin-wall metal or plastic tubing. No jackets were used in the tests for tensile strength. In the P-V tests, the quasi-hydrostatic pressure medium (tin) encapsulated the sample. The samples for ultrasonic velocity determination were jacketed using Scotch cast resin. All experiments were carried out at strain rates of  $10^{-4}$  to  $10^{-5}$  s<sup>-1</sup>.

### 3. RESULTS

#### 3.1 Pressure-volume

The P-V behavior was determined for units B, C and D only, in the stress state indicated in Fig. 1a. We were unable to prepare adequate test sample material from unit A because of excessive bedding plane fracturing during the specimen coring operation. In Figure 2, we summarize the P-V behavior of these three units up to 4.0 GPa, about the practical limit for the apparatus.

Also indicated here is the average dry density, ( $\rho$ ), and the depth of test samples. This figure clearly indicates that the brown gaseous shale member is the most compressible (except at low pressure), followed by the Marcellus black shale member and the Olentangy white shale member. Volume changes at 2.1 GPa, for example, are about 9.2%, 8.3%, and 6.5%, respectively for the three members. Each curve shown in Fig. 2 is based on the average of three or more tests.

Comparison of values for bulk moduli calculated at 0.5 GPa indicated that the Brown member is lowest (18 GPa) followed by the Black (22 GPa) and the Olentangy (31 GPa). At 4 GPa, the relative order changes: Brown = 61, Olentangy = 64 and Black = 73 GPa.

We tested Unit C both parallel and perpendicular to bedding to make sure our P-V technique would yield similar results independent of sample orientation. Both sets of tests agreed within the experimental error and thus we believe the technique is valid and the results in Fig. 2 should reflect the P-V behavior of the three units, independent of orientation.

### 3.2 Triaxial Stress Loading in Compression

Each of the four units A, B, C, and D was tested to failure in triaxial compression at confining pressures ranging to 300 MPa (Fig. 1a). The strength behavior was determined both parallel and perpendicular to bedding for each material. In each case at low to moderate pressures, the failure mode is termed brittle in all samples and is the result of combined tensile and shear fracture. The former dominates at the lower pressure and is oriented parallel to  $\sigma_1$ . However, the latter becomes dominant at moderate-high pressures and is oriented at  $\sim 30^\circ$  to  $\sigma_1$ . At the highest pressures tested, these shale units frequently become ductile; that is, all deformation is quasi-uniformly distributed within the test sample. The brittle-ductile transition point usually occurs at lower pressures for loading perpendicular to bedding than for compression parallel to it. Results are reported in Figures 3 to 6 in the form of stress difference (strength),  $\sigma_1 - \sigma_3$ , versus  $\sigma_2$  (confining pressure). All data are summarized in Tables 1-4. In each figure, the compression failure envelope for the virgin shale is defined by the points O from each test. Also shown in these figures is the post-failure strength envelope, designated by  $\Delta$ . This lower surface delineates the strength of the fractured shale vs. confining pressure. At the brittle-ductile transition, there is no strength decrease upon failure, only distributed flow; and hence, the two curves become identical at higher pressure. The brittle-ductile transition is indicated on Figures 3-6 either by a full arrow ( $\rightarrow$ ) if the value is well circumscribed, or by a dashed arrow ( $- - \rightarrow$ ) if the estimate has a larger uncertainty.

In intercomparing Figures 3-6, several trends emerge:

- . Unit A in either orientation is strongest at all pressures, followed by units D, B, and C in decreasing order of strength,
- . at all pressures, both orientations of Unit A are brittle while those of unit B are ductile,
- . the  $\perp$  orientation becomes ductile at high pressure for units C, D while the  $\parallel$  orientation remains brittle in both of these cases,

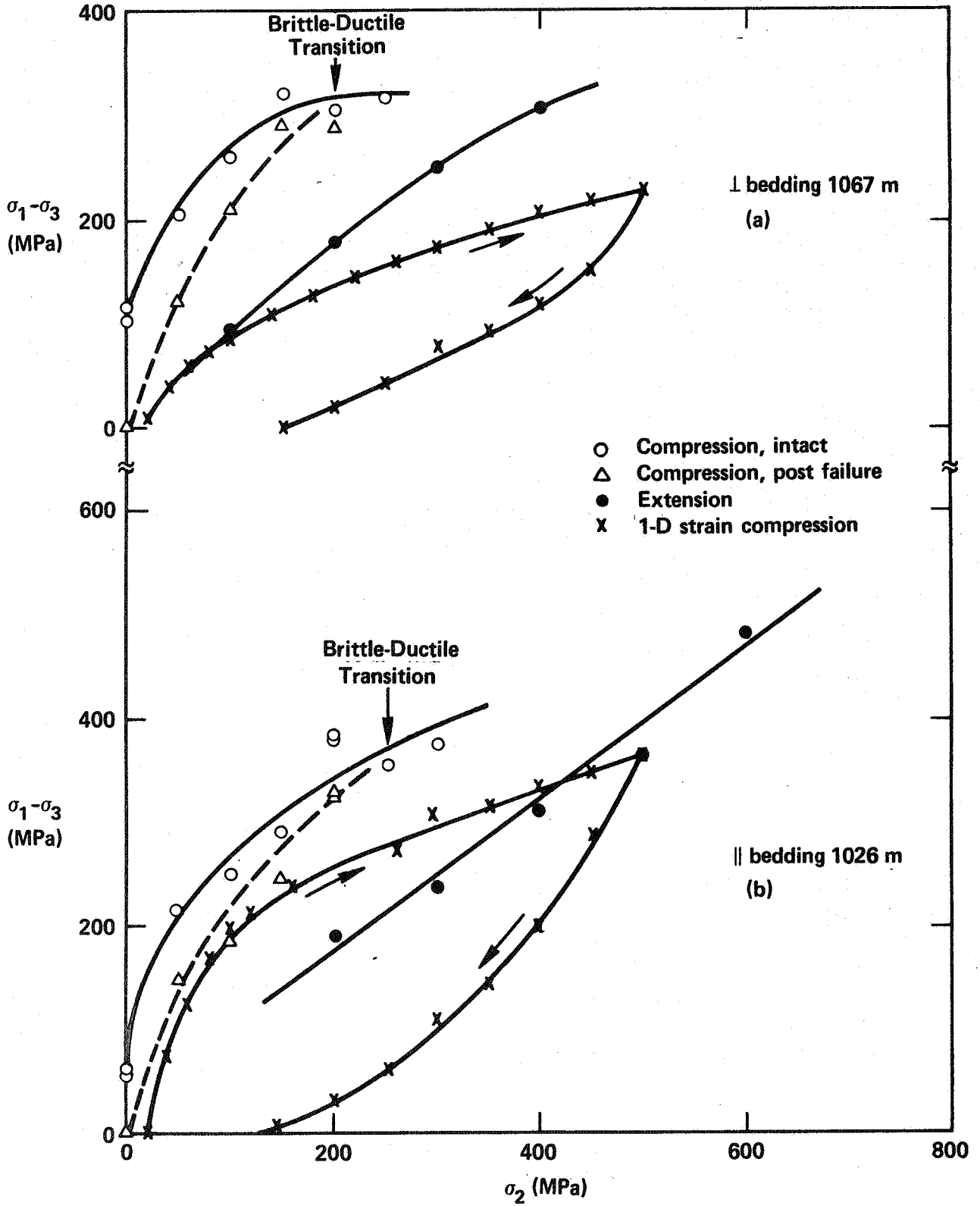


Figure 4: Failure Envelopes,  $\sigma_1 - \sigma_3$  Versus  $\sigma_2$  (Pressure). Brown Gaseous Shale (Unit B).

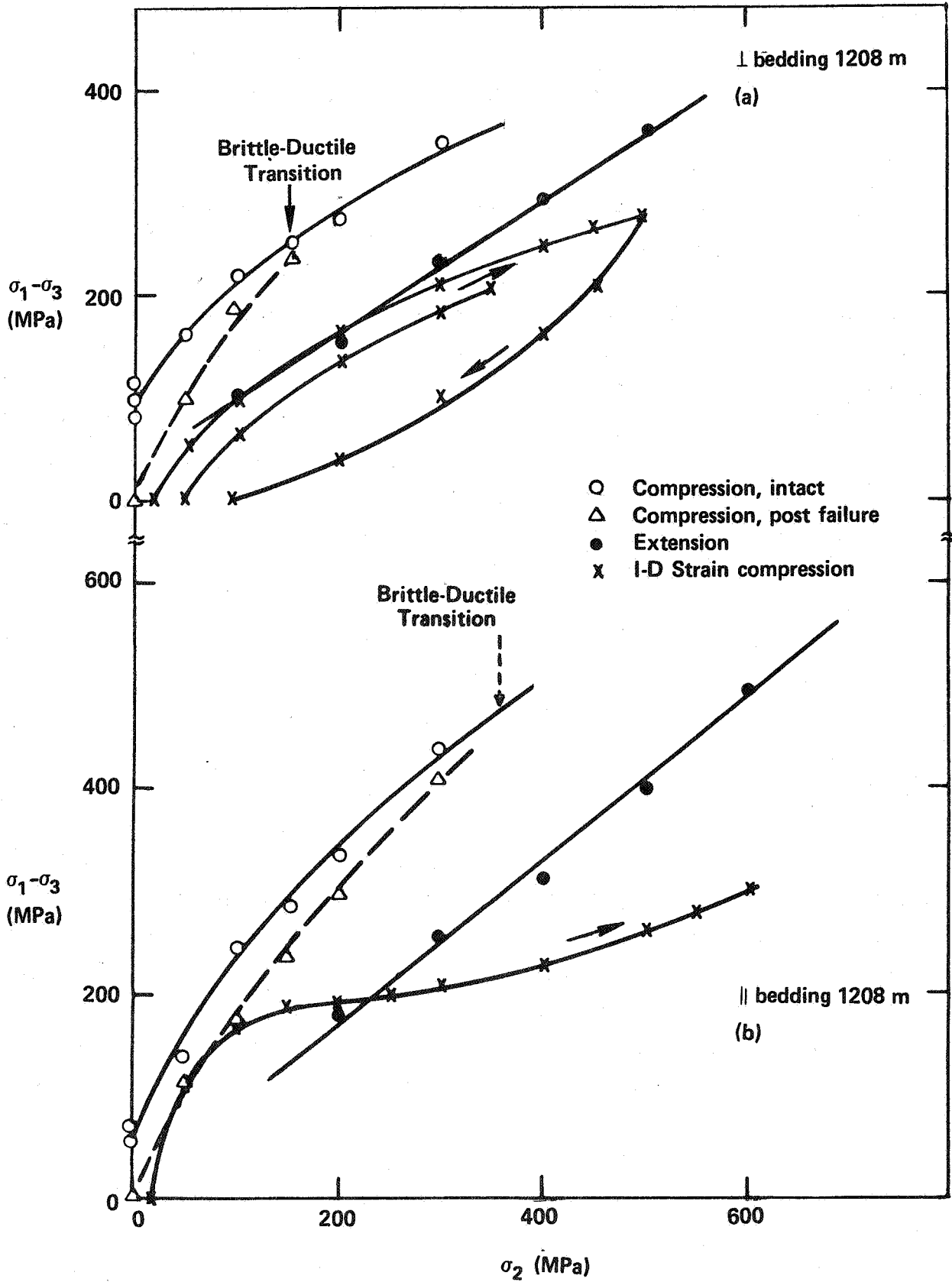


Figure 6: Failure Envelopes,  $\sigma_1 - \sigma_3$  Versus  $\sigma_2$  (Pressure). Marcellus Black Shale (Unit D).

as  $\sigma_1$  increased (Fig. 4, 6). Because  $\epsilon_2$  was not determined, it was not possible to assess how closely 1-D strain loading was approximated. We have performed a limited number of these tests on units B, C, and D with the loading direction being both  $\parallel$  and  $\perp$  to bedding in most cases. No work was done on Unit A because of difficulty in preparing suitable test samples. All results have been summarized in Tables 2 to 4. The various loading/unloading paths in 1-D strain are shown in Figures 4a, b, 5a and 6a, b for comparison with the failure envelopes in both compression as well as extension. In each case, there is a very large hysteresis between the loading and unloading paths, a common characteristic of this stress state (15-17). In loading  $\perp$  to bedding for each material (Fig. 4a, 5a, 6a), the stress path generally appears to follow the extension failure envelope to low-moderate pressure, then to progressively deviate towards lower shear stress at high pressure. For the two cases parallel to bedding (Fig. 4b, 6b) the loading path rises steeply to a shear stress noticeably above the extension envelope at low pressure, then crosses it to a lower shear stress at moderate-high pressure. In two other rock types, Westerly granite and Blair dolomite--both quite different materials but admittedly isotropic, the 1-D strain loading path closely follows the extension failure envelope (15,18-20). This suggests that behavior in these stress states may be related for at least these two rocks and perhaps in those Devonian shale members as well. In units B and D (Figs. 4 and 6), the 1-D loading path remains lower ( $\sim 1/2$  the level) than the failure envelope in compression at low-moderate pressure, then increasingly deviates at high pressure. This behavior is similar to that of many other rocks investigated in this Laboratory (13,21-23). In those studies it was suggested that the 1-D loading path closely approximates the onset for dilatancy. The present data (except for Unit C, Fig. 5a), including the extension data discussed above, is consistent with that hypothesis. In Figure 5a, the 1-D strain loading becomes anomalous at high pressure where it can be seen that the path rises above the compression failure envelope. We are at a loss to explain this behavior and are not aware of any other experimental results on any rock where this has been observed. It may be related to the fact that the extension envelope also lies above that for compression, also an anomaly which was noted above.

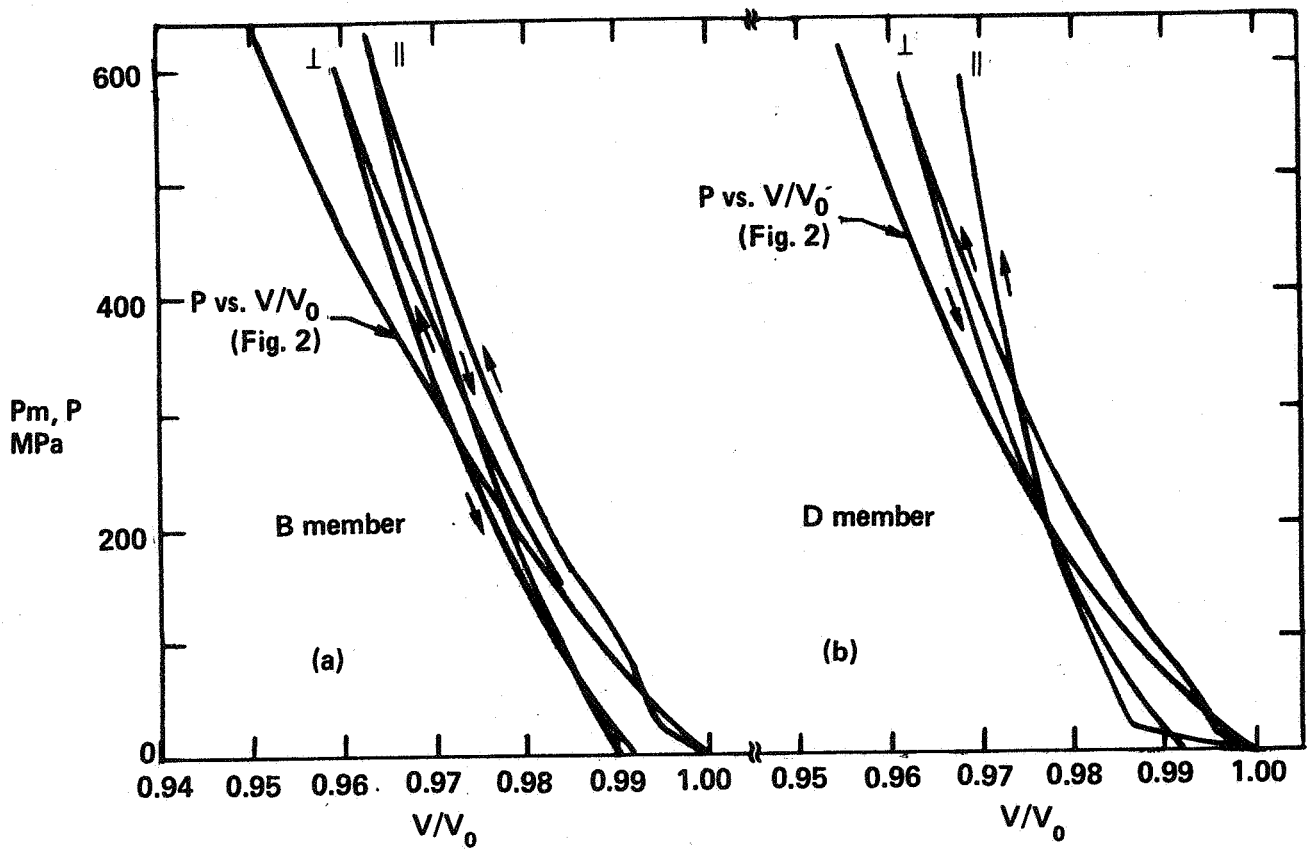


Figure 7: Mean Stress,  $P_m$ , Versus  $V/V_0$ , for 1-D Strain Loading/Unloading ⊥ and || Bedding for Brown Gaseous Shale Unit B (7a) and Marcellus Black Shale Unit D (7b).

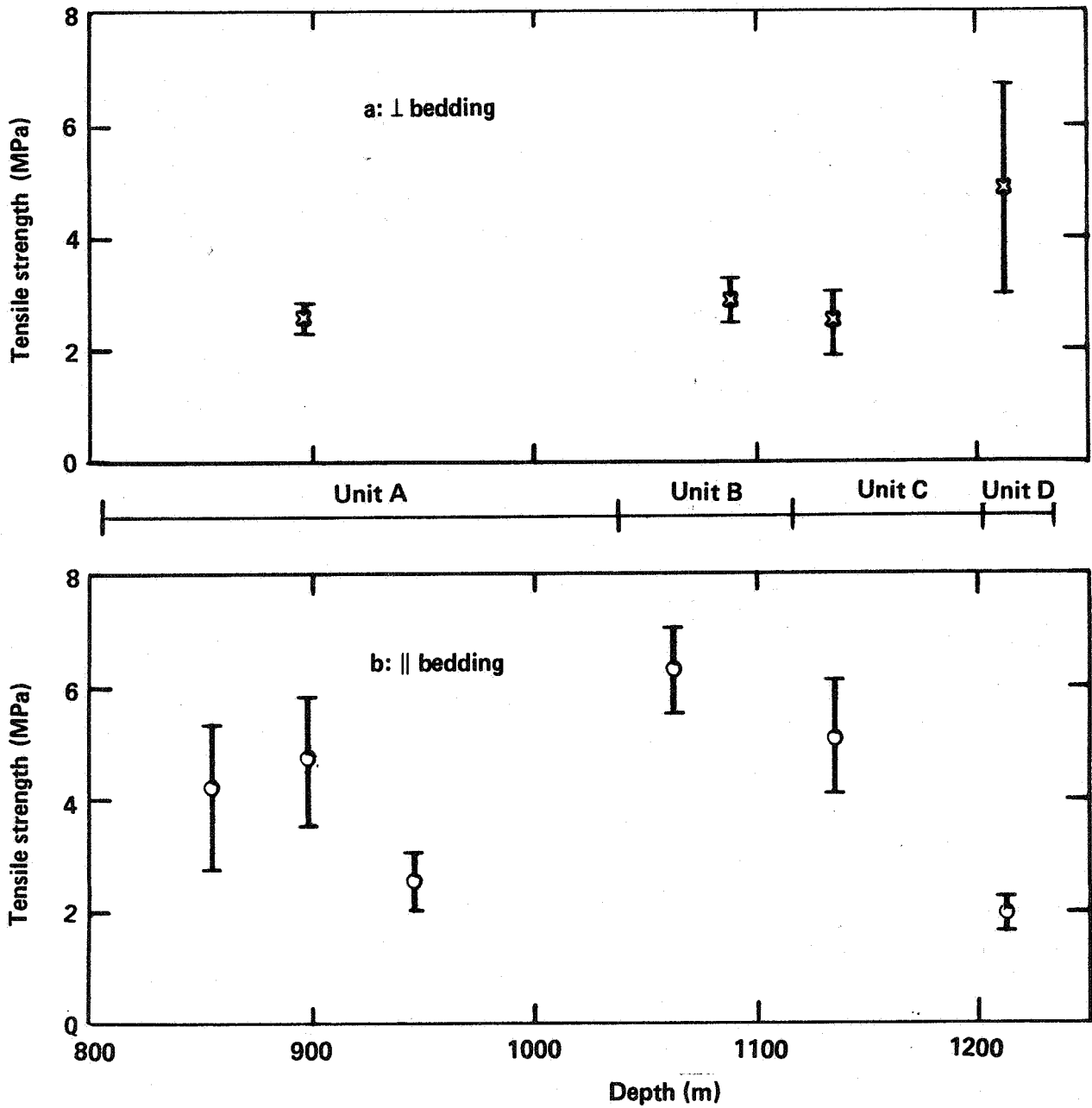


Figure 8: Tensile Strength as Determined by the Indirect (Brazilian) Test for Shale Units A, B, C, and D.

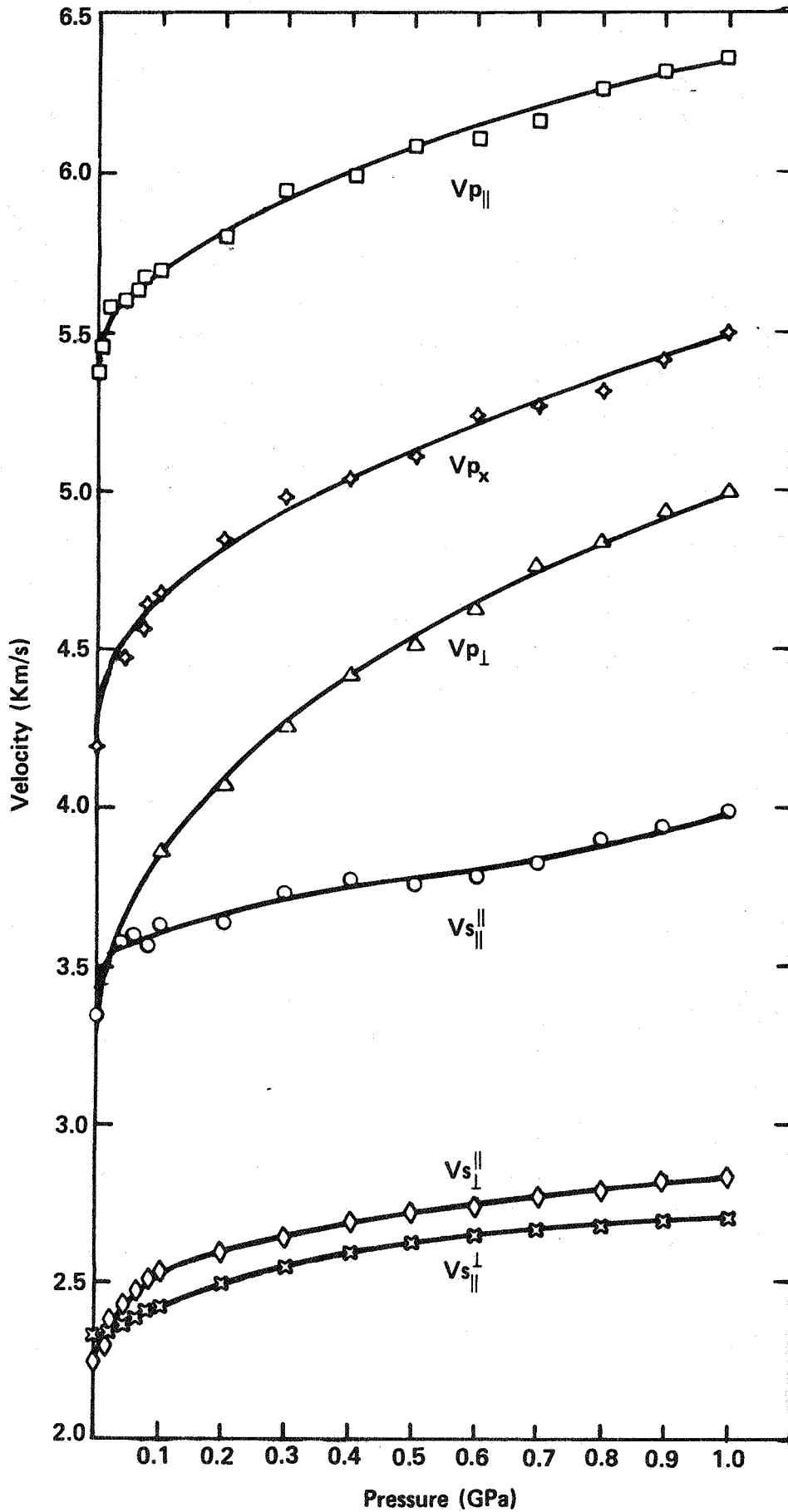


Figure 9: Velocity-Pressure Plot of Olentangy Shale (Unit C), 1195 m.

where  $\rho$  is the bulk density of the sample. The other coefficients are zero. With our velocity data, the relationships  $C_{11} = C_{22}$ ,  $C_{44} = C_{55}$ , and  $C_{23} = C_{13}$  can not be quantitatively tested. However, the specimens parallel to bedding and at  $45^\circ$  to bedding were randomly cored from larger samples and the velocities of a wave mode determined from these specimens do not differ by more than 5%, as was mentioned earlier. In calculating  $C_{44}$ , we have used the mean value of  $v_{s\perp}^{\parallel}$  and  $v_{s\parallel}^{\perp}$ . Due to the nature of the relation between elastic stiffness and velocity, the uncertainties of the calculated elastic moduli are greater than those of velocities by about 10%. Table 10 summarizes the elastic stiffness of the four shale units. Although we only list the bulk density at room conditions  $\rho_0$ , in the calculation of the stiffness coefficients, we took account the increase of bulk density due to compression. In Figure 10, we illustrate one example of these stiffness coefficients for the same shale unit (Unit C) whose velocities were shown in Fig. 9. Young's moduli ( $E_x$ ,  $E_y$ , and  $E_z$ ), shear moduli ( $G_{xz}$ ,  $G_{yz}$ , and  $G_{xy}$ ), Poisson's ratios ( $\nu_{xy}$ ,  $\nu_{xz}$ , and  $\nu_{zx}$ ) can be calculated from the stiffness coefficients as:

$$\begin{aligned} E_x &= E_y = 1/S_{11} \\ E_z &= 1/S_{33} \\ G_{xz} &= G_{yz} = 1/S_{44} \\ G_{xy} &= E_x / 2(1 + \nu_{xy}) \\ \nu_{xy} &= -S_{12} / S_{11} \\ \nu_{xz} &= -S_{13} / S_{11} \\ \nu_{zx} &= E_x \nu_{xz} / E_x \end{aligned}$$

where

$$\begin{aligned} S_{11} &= (C_{11}C_{33} - C_{13}^2) / D \\ S_{33} &= 4C_{66}(C_{11} - C_{66}) / D \\ S_{44} &= 1/C_{44} \\ S_{12} &= [C_{13}^2 - (C_{11} - 2C_{66})C_{33}] / D \\ S_{13} &= -2C_{13}C_{66} / D \end{aligned}$$

and

$$D = 4C_{66}^2 [C_{33}(C_{11} - C_{66}) - C_{13}^2]$$

Each of the four shale units tested have similar independent elastic stiffness except  $C_{11}$  and  $C_{66}$ . Unit A has a much greater value for  $C_{11}$  than the others while in Unit C, both  $C_{11}$  and  $C_{66}$  are much larger. The bulk density of units A and C are significantly greater than that of B and D (Table 10). The two elastic stiffness coefficients  $C_{11}$  and  $C_{66}$  would be expected to show the least effect of any microcracks or micaceous minerals along the bedding plane.

Table 1: Upper Gray Shale, Unit A

Triaxial Stress, Compression  $\perp$  Bedding, 898 m

$\sigma_1$	$\sigma_1^*$	$\sigma_2 = \sigma_3$	$\sigma_1 - \sigma_3$	$(\sigma_1 - \sigma_3)^*$	Remarks
40	0.1	0.1	40	0	Brittle
97	0.1	0.1	97	0	Brittle
150	0.1	0.1	150	0	Brittle
376	269	50	326	219	Brittle
558	426	100	458	326	Brittle
717	573	150	567	423	Brittle
794	702	200	594	502	Brittle
1027	951	300	727	651	Brittle

Triaxial Stress, Extension  $\perp$  Bedding, 950 m

$\sigma_1 = \sigma_2$	$\sigma_3$	$\sigma_3^*$	$\sigma_1 - \sigma_3$	$(\sigma_1 - \sigma_3)^*$	Remarks
100	13	100	87	0	Brittle
100	6	100	94	0	Brittle
200	44	200	156	0	Brittle
300	64	300	236	0	Brittle
400	116	400	284	0	Brittle
500	161	500	339	0	Brittle

Triaxial Stress, Compression  $\parallel$  Bedding, 898 m

$\sigma_1$	$\sigma_1^*$	$\sigma_2 = \sigma_3$	$\sigma_1 - \sigma_3$	$(\sigma_1 - \sigma_3)^*$	Remarks
47	0.1	0.1	47	0	Brittle
115	0.1	0.1	115	0	Brittle
76	0.1	0.1	76	0	Brittle
277	173	50	227	123	Brittle
443	397	100	343	297	Brittle
484	433	150	334	283	Brittle
577	541	200	377	341	Brittle
750	733	300	450	433	Brittle

Triaxial Stress, Extension  $\parallel$  Bedding, 950 m

$\sigma_1 = \sigma_2$	$\sigma_3$	$\sigma_3^*$	$\sigma_1 - \sigma_3$	$(\sigma_1 - \sigma_3)^*$	Remarks
200	10	200	190	0	Brittle
300	34	300	266	0	Brittle
400	78	400	322	0	Brittle
405	118	405	287	0	Brittle
500	69	500	431	0	Brittle
609	106	609	503	0	Brittle
779	132	779	647	0	Brittle

\*Post fracture

All stress values in MPa

Table 2 (Cont.): Brown Gaseous Shale, Unit B

Triaxial Stress, Compression || Bedding, 1047 m

$\sigma_1$	$\sigma_1^*$	$\sigma_2 = \sigma_3$	$\sigma_1 - \sigma_3$	$(\sigma_1 - \sigma_3)^*$	Remarks
59	0.1	0.1	59	0	Brittle
56	0.1	0.1	56	0	Brittle
265	197	50	215	147	Brittle
350	289	100	250	189	Brittle
440	396	150	290	246	Brittle
580	525	200	380	325	Brittle
582	523	200	382	323	Brittle
605	--	250	355	--	Transitional
675	--	300	375	--	Ductile

Triaxial Stress, Extension || Bedding, 1026 m

$\sigma_1 = \sigma_2$	$\sigma_3$	$\sigma_3^*$	$\sigma_1 - \sigma_3$	$(\sigma_1 - \sigma_3)^*$	Remarks
200	10	200	190	0	Brittle
300	64	300	236	0	Brittle
400	87	400	313	0	Brittle
500	134	500	366	0	Brittle
600	118	600	482	0	Brittle

Quasi Uniaxial Strain, Compression || Bedding, 1047 m

$\sigma_1$	$\sigma_3 = \sigma_2$	$\sigma_1 - \sigma_3$	Remarks
81	76	5	Loading
150	125	25	Loading
260	150	110	Loading
328	200	128	Loading
418	250	168	Loading
510	300	210	Loading
650	400	250	Loading
764	500	264	Loading
20	20	0	Loading
116	40	76	Loading
186	60	126	Loading
250	80	170	Loading
296	100	196	Loading
332	120	212	Loading
400	160	240	Loading
534	260	274	Loading
600	300	300	Loading
668	350	318	Loading
734	400	334	Loading
800	450	350	Loading
868	500	368	Loading
738	450	288	Unloading
596	400	196	Unloading
494	350	144	Unloading
412	300	112	Unloading
312	250	62	Unloading
232	200	32	Unloading
153	145	8	Unloading

\*Post fracture  
All stress values in MPa

Table 3 (Cont.): Olentangy White Shale, Unit C

$\sigma_1$	$\sigma_3=\sigma_2$	$\sigma_1-\sigma_3$	Remarks
50	40	10	Loading
160	80	80	Loading
244	120	124	Loading
360	180	180	loading
428	220	208	Loading
490	260	230	Loading
550	300	250	Loading
606	340	266	Loading
664	380	284	Loading
720	420	300	Loading
774	460	314	Loading
830	500	330	Loading
672	440	232	Unloading
550	380	170	Unloading
426	320	106	Unloading
360	280	80	Unloading
290	240	50	Unloading
230	200	30	Unloading
174	160	14	Unloading
135	135	0	Unloading

Triaxial Stress, Compression || Bedding, 1134 m

$\sigma_1$	$\sigma_1^*$	$\sigma_2 = \sigma_3$	$\sigma_1 - \sigma_3$	$(\sigma_1 - \sigma_3)^*$	
21	0.1	0.1	21	0	Brittle
32	0.1	0.1	32	0	Brittle
123	0.1	50	73	0	Brittle
202	177	100	102	77	Brittle
274	254	150	124	104	Brittle
412	403	250	162	153	Brittle
481	475	300	181	175	Brittle

Triaxial Stress, Extension || Bedding, 1173 m

$\sigma_1 = \sigma_2$	$\sigma_3$	$\sigma_3^*$	$\sigma_1 - \sigma_3$	$(\sigma_1 - \sigma_3)^*$	
101	-6	101	107	0	Brittle
200	30	200	170	0	Brittle
300	63	300	237	0	Brittle
400	96	400	304	0	Brittle

\*Post fracture  
All stress values in MPa

Table 4 (Cont.): Marcellus Black Shale, Unit D (Cont.)

Triaxial Stress, Compression || Bedding, 1207 m

$\sigma_1$	$\sigma_1^*$	$\sigma_2 = \sigma_3$	$\sigma_1 - \sigma_3$	$(\sigma_1 - \sigma_3)^*$	Remarks
70	0.1	0.1	70	0	Brittle
58	0.1	0.1	58	0	Brittle
228	166	50	178	116	Brittle
342	271	100	242	171	Brittle
436	385	150	286	235	Brittle
534	499	200	334	299	Brittle
739	710	300	439	410	Brittle

Triaxial Stress, Extension || Bedding, 1208 m

$\sigma_1 = \sigma_2$	$\sigma_3$	$\sigma_3^*$	$\sigma_1 - \sigma_3$	$(\sigma_1 - \sigma_3)^*$	Remarks
200	18	200	182	0	Brittle
300	46	300	254	0	Brittle
400	89	400	311	0	Brittle
500	104	500	396	0	Brittle
600	105	600	495	0	Brittle

Quasi Uniaxial Strain, Compression || Bedding, 1216 m

$\sigma_1$	$\sigma_3 = \sigma_2$	$\sigma_1 - \sigma_3$	Remarks
20	20	0	Loading
164	50	114	Loading
268	100	168	Loading
340	150	190	Loading
388	198	190	Loading
450	250	200	Loading
511	303	208	Loading
630	400	230	Loading
760	500	260	Loading
825	550	275	Loading
902	600	302	Loading

\*Post fracture  
All stress values in MPa

Table 10

## Sonic Velocities

Rock Unit (Depth)	Pressure (GPa)	(km/s)												
		$V_{P\perp}$	$\tilde{V}_{P\perp}$	$V_{P\parallel}$	$\tilde{V}_{P\parallel}$	$V_{P\perp}$	$\tilde{V}_{P\perp}$	$V_{P\parallel}$	$\tilde{V}_{P\parallel}$	$V_{S\perp}$	$\tilde{V}_{S\perp}$	$V_{S\parallel}$	$\tilde{V}_{S\parallel}$	
A (867m)	0.0001	3.07	1.0	5.0	1.63	--	--	--	--	--	3.07	1.0	2.20	0.72
	0.01	3.77	1.23	5.13	1.67	--	--	--	--	--	3.10	1.01	2.35	0.77
	0.02	3.84	1.25	5.14	1.67	--	--	--	--	--	3.11	1.01	2.40	0.78
	0.04	3.93	1.28	5.21	1.70	--	--	--	--	--	3.13	1.02	2.45	0.80
	0.06	4.02	1.31	5.28	1.72	--	--	--	--	--	3.15	1.03	2.50	0.81
	0.08	4.13	1.35	5.30	1.73	--	--	--	--	--	3.17	1.03	2.56	0.83
	0.10	4.20	1.37	5.35	1.74	--	--	--	--	--	3.19	1.04	2.58	0.84
	0.20	4.35	1.42	5.50	1.79	--	--	--	--	--	3.25	1.06	2.69	0.88
	0.30	4.43	1.44	5.59	1.82	--	--	--	--	--	3.30	1.07	2.74	0.89
	0.40	4.52	1.47	5.68	1.85	--	--	--	--	--	3.34	1.09	2.78	0.91
	0.50	4.59	1.50	5.72	1.86	--	--	--	--	--	3.36	1.09	2.82	0.92
	0.60	4.69	1.53	5.79	1.89	--	--	--	--	--	3.40	1.11	2.85	0.93
	0.70	4.77	1.55	5.82	1.90	--	--	--	--	--	3.43	1.12	2.88	0.94
	0.80	4.81	1.57	5.85	1.91	--	--	--	--	--	3.45	1.12	2.89	0.94
	0.90	4.87	1.59	5.91	1.93	--	--	--	--	--	3.47	1.13	2.91	0.95
	1.00	4.90	1.60	5.99	1.95	--	--	--	--	--	3.48	1.13	2.93	0.95

Table 10 (Continued)

Rock Unit (Depth)	Pressure (GPa)	(km/s)											
		$V_{P\perp}$	$\tilde{V}_{P\perp}$	$V_{P\parallel}$	$\tilde{V}_{P\parallel}$	$V_{P_X}$	$\tilde{V}_{P_X}$	$V_{S\perp}$	$\tilde{V}_{S\perp}$	$V_{S\parallel}$	$\tilde{V}_{S\parallel}$	$V_{S\perp}$	$\tilde{V}_{S\perp}$
C (1195 m)	0.0001	3.24	1.00	5.37	1.66	4.16	1.28	2.30	0.71	3.33	1.03	2.25	0.69
	0.01	3.44	1.06	5.48	1.69	4.38	1.35	2.32	0.72	3.47	1.07	2.30	0.71
	0.02	3.53	1.10	5.56	1.72	4.43	1.37	2.33	0.72	3.51	1.08	2.34	0.72
	0.04	3.64	1.12	5.58	1.72	4.49	1.39	2.35	0.73	3.55	1.10	2.40	0.74
	0.06	3.73	1.15	5.62	1.73	4.55	1.40	2.38	0.73	3.57	1.10	2.46	0.76
	0.08	3.79	1.17	5.67	1.75	4.63	1.43	2.40	0.74	3.57	1.10	2.49	0.77
	0.10	3.86	1.19	5.69	1.76	4.67	1.44	2.41	0.74	3.61	1.11	2.52	0.78
	0.20	4.08	1.26	5.81	1.79	4.85	1.50	2.50	0.77	2.65	1.13	2.61	0.81
	0.30	4.26	1.31	5.94	1.83	4.98	1.54	2.55	0.79	3.71	1.14	2.65	0.82
	0.40	4.42	1.36	6.00	1.85	5.04	1.56	2.60	0.80	3.75	1.16	2.68	0.83
	0.50	4.53	1.40	6.08	1.88	5.12	1.58	2.63	0.81	3.77	1.16	2.72	0.84
	0.60	4.65	1.44	6.12	1.89	5.23	1.61	2.65	0.82	3.80	1.17	2.74	0.85
	0.70	4.76	1.47	6.18	1.91	5.28	1.63	2.67	0.82	3.84	1.19	2.77	0.85
	0.80	4.83	1.49	6.25	1.93	5.32	1.64	2.68	0.83	3.89	1.20	2.79	0.86
	0.90	4.92	1.52	6.31	1.95	5.42	1.67	2.70	0.83	3.93	1.21	2.82	0.87
	1.00	4.98	1.54	6.35	1.96	5.50	1.69	2.71	0.84	3.97	1.23	2.84	0.88

Table 10: Elastic Stiffness Coefficients of Devonian Shale Units A-D as a Function of Pressure

Sample	Depth	Pressure	$C_{11}(=C_{22})$	$C_{33}$	$C_{44}(=C_{55})$	$C_{66}$	$C_{13}(=C_{23})$
Unit	Range (m)	(GPa)	(GPa)	(GPa)	(GPa)	(GPa)	(GPa)
A $\rho_0 = 2.71$ Mg/m <sup>3</sup>	867	10 <sup>-4</sup>	67.7	25.5	13.2	25.5	--
		0.01	71.1	38.6	15.1	26.0	--
		0.02	71.2	39.9	15.5	26.1	--
		0.04	73.9	41.9	16.4	26.6	--
		0.06	75.7	43.9	16.8	27.1	--
		0.08	76.7	46.7	17.7	27.1	--
		0.10	77.7	48.1	18.1	27.8	--
		0.20	81.7	51.9	19.9	28.9	--
		0.30	85.6	53.7	20.5	29.6	--
		0.40	88.8	56.1	21.5	30.9	--
		0.50	90.1	58.5	22.1	30.9	--
		0.60	93.2	61.2	22.5	32.2	--
		0.70	94.5	62.9	23.1	32.9	--
		0.80	95.7	64.6	23.2	32.9	--
0.90	97.9	66.5	23.7	33.5	--		
1.00	100.2	67.4	23.8	33.6	--		
B $\rho_0 = 2.56$ Mg/m <sup>3</sup>	1041	10 <sup>-4</sup>	58.2	31.5	12.6	20.9	18.4
		0.01	59.8	32.7	13.3	23.8	19.8
		0.02	60.6	33.8	14.4	24.3	19.0
		0.04	61.5	35.7	14.8	24.8	19.5
		0.06	62.4	37.5	14.8	24.8	19.9
		0.08	63.4	38.2	15.2	25.4	20.4
		0.10	64.2	38.8	15.3	25.5	21.6
		0.20	67.3	43.1	16.2	26.7	24.6
		0.30	72.3	46.7	16.8	28.0	27.0
		0.40	74.2	49.8	17.7	28.7	26.8
		0.50	76.4	54.5	17.8	29.4	30.6
		0.60	79.5	57.1	19.2	29.6	32.8
		0.70	80.7	58.8	21.2	30.3	30.1
		0.80	82.0	63.8	21.7	31.0	33.3
0.90	84.1	65.8	22.2	31.1	32.4		
1.00	85.3	67.5	22.8	31.2	32.0		

5. REFERENCES

1. Heuze, F.E. (1986) "The Unconventional Gas Program at Lawrence Livermore National Laboratory", UCID-20610, January.
2. Report of the Natural Gas Technology Task Force for the Technical Advisory Committee of the Natural Gas Survey by the Federal Power Commission (1975).
3. Swift, R.P. (1984) "A Perspective on Modeling Tailored-Pulse Loading (TPL) for Borehole Stimulation", Lawrence Livermore National Laboratory, UCID-20147, August.
4. Cuderman, J.F. (1984) "High-Energy Gas Fracturing Development", Sandia National Laboratories, Albuquerque, SAND 84-0247, June.
5. Cuderman, J.F. (1986) "Proceedings of Tailored-Pulse Fracturing Meeting", Albuquerque, NM, Dec. 4-5, 1985. Draft report from Sandia National Laboratories.
6. Taylor, L.M., Swenson, D.V., and Cooper, P.W. (1984) "A Coupled Gas Flow Solid Dynamics Model for Predicting the Formation of Fracture Patterns in Gas Well Stimulation Experiments", Sandia National Laboratories, Albuquerque, SAND 84-0016, July.
7. Hanson, H.M., Schmidt, R.A., Cooley, C.H., and Schatz, J.F. (1984) "Multiple Fracture Stimulation Using Controlled Pulse Pressurization", SPE/DOE/GRI 12839, Unconventional Gas Recovery Symposium, Pittsburgh, PA, May (SPE, Dallas, TX).
8. Nilson, R.H., Proffer, W.J., and Duff, R.E. (1985) "Modelling of Gas-Driven Fractures Induced by Propellant Combustion in Boreholes", Int. J. Rock Mechanics and Mining Science, v. 22, n. 1, pp 3-19.
9. Stephens, D.R., Lilley, E.M., and Louis, H. (1970) "Pressure-Volume Equation of State of Consolidated and Fractured Rocks to 40 Kb", Int. J. Rock Mech. Min. Sci. 7, 257-296.
10. Stephens, D.R., and Lilley, E.M. (1971) "Pressure-Volume Properties of Two Apollo 12 Basalts", Geochem. et Cosmochim. Acta, Supply. 2 3, 2165-2176.
11. Handin, J. and Hager, R.V. (1957) "Experimental Deformation of Sedimentary Rocks under Confining Pressure: Tests at Room Temperature on Dry Samples", Amer. Assoc. Petrol. Geol. Bull., v. 41, n. 1.
12. Heard, H.D., (1960) "Transition from Brittle to Ductile Flow in Solenhofen Limestone as a Function of Temperature, Confining Pressure, and Interstitial Fluid Pressure", in Rock Deformation, Memoir 79, ed, by D. T. Griggs and J. Handin (Geol. Soc. Am., Boulder, Colo., 1960) Ch.7, p. 193.
13. Schock, R.N., Heard, H.C., and Stephens, D.R. (1973) "Stress-Strain Behavior of a Grandiorite and Two Greywackes on Compression to 20 Kb", Jour. Geophys. Res., 78, 5922.

REFERENCES (Cont.)

28. Weiss, L. E., (1968) "Flexural Slip Folding of Foliated Model Materials", p. 294 in Kirk Bands and Brittle Deformation, A. J. Baer and D. K. Narres Eds., Geol. Soc. Canada paper 68-52.
29. Birch, F., (1960) "The Velocity of Compressional Waves in Rocks to 10 Kilobars", Part I, Jour. Geophys. Res. 65, 1083.
30. Schock, R. N., Louis, H., and Lilley, E.M. (1969) "The Determination of Acoustic Velocities and Dynamic Elastic Moduli in Rocks Under Pressure", Lawrence Livermore National Laboratory Report UCRL-50750.
31. Nye, J. F. (1960) Physical Properties of Crystals, Oxford.
32. McSkimin, H.J. (1964) "Ultrasonic Method for Measurement" in Physical Acoustics, W. P. Mason ed., Vol. 1, Part A, Academic Press, New York.

6. ACKNOWLEDGMENTS

This work was performed as part of the Unconventional Gas Program of the Lawrence Livermore National Laboratory, Livermore, CA. It was funded by the U. S. Department of Energy, Morgantown Energy Technology Center, under contract W-7405-ENG-48.

The authors acknowledge the constructive comments of A. Duba and F. Heuze, at LLNL, and C. Komar and A. Yost, at METC.